

Lawrence Berkeley National Laboratory

Recent Work

Title

ATOMIC MECHANISMS OF PRECIPITATE PLATE GROWTH IN THE Al-Ag SYSTEM - II. HIGH-RESOLUTION TRANSMISSION ELECTRON MICROSCOPY

Permalink

<https://escholarship.org/uc/item/3qt1f9b0>

Authors

Howe, J.M.

Aaronson, H.I.

Gronsky, R.

Publication Date

1984-09-01



Lawrence Berkeley Laboratory

UNIVERSITY OF CALIFORNIA

Materials & Molecular Research Division

Submitted to Acta Metallurgica

ATOMIC MECHANISMS OF PRECIPITATE PLATE GROWTH IN
THE Al-Ag SYSTEM - II. HIGH-RESOLUTION
TRANSMISSION ELECTRON MICROSCOPY

J.M. Howe, H.I. Aaronson, and R. Gronsky

September 1984

RECEIVED
LAWRENCE
BERKELEY LABORATORY
NOV 20 1984
LIBRARY AND
DOCUMENTS SECTION

For Reference
Not to be taken from this room



LBL-16504
c.1

DISCLAIMER

This document was prepared as an account of work sponsored by the United States Government. While this document is believed to contain correct information, neither the United States Government nor any agency thereof, nor the Regents of the University of California, nor any of their employees, makes any warranty, express or implied, or assumes any legal responsibility for the accuracy, completeness, or usefulness of any information, apparatus, product, or process disclosed, or represents that its use would not infringe privately owned rights. Reference herein to any specific commercial product, process, or service by its trade name, trademark, manufacturer, or otherwise, does not necessarily constitute or imply its endorsement, recommendation, or favoring by the United States Government or any agency thereof, or the Regents of the University of California. The views and opinions of authors expressed herein do not necessarily state or reflect those of the United States Government or any agency thereof or the Regents of the University of California.

Atomic Mechanisms of Precipitate Plate Growth in the Al-Ag System - II. High-Resolution Transmission Electron Microscopy

J.M. Howe, H.I. Aaronson* and R. Gronsky

Materials and Molecular Research Division
Lawrence Berkeley Laboratory
Department of Materials Science and Mineral Engineering
University of California, Berkeley, CA 94720

ABSTRACT

High-resolution electron microscopy was used to study the interfacial structure of γ' precipitates in an Al-15 w/o Ag alloy aged at 350°C. The results of these studies show that: (1) all ledges are multiples of two {111} planes high, supporting the theory and conventional transmission electron microscopy observations that plate thickening occurs by passage of Shockley partial dislocations on alternate {111} planes, (2) most ledges are more than just two planes high, indicating a strong tendency toward diffusional and/or elastic interactions, (3) the terraces between ledges are atomically flat and ledges are uniformly stepped-down from the centers to the edges of isolated precipitates as predicted by the general theory of precipitate morphology, (4) the {111} planes are continuous across the edges of ledges, indicating that they are largely coherent and not disordered as treated in most kinetic analyses, and (5) the edges of precipitate plates appear to be composed of similar two-plane ledges arranged vertically above one another and hence, may grow by the same mechanism of atomic attachment as ledges on the broad faces. Examination of γ' plates during early stages of growth indicates that their aspect ratio may deviate from the equilibrium value almost

immediately, probably due to the ledge mechanism of growth. Lastly, an atomic model of a γ' precipitate was used to test the high-resolution images obtained, and illustrate possible atomic growth mechanisms of the ledges.

1. INTRODUCTION

Part I of this study presented the results of a conventional transmission electron microscopy (CTEM) investigation of precipitate plates in an Al-15 w/o Ag alloy. Shockley partial dislocation ledges on the faces of precipitates were sometimes found to interact sufficiently to create multiple-unit ledges, displaying the diffraction contrast behavior of perfect $1/2 \langle 110 \rangle$ dislocations. In addition, observations of the morphology of precipitate edges revealed similarities between the growth of ledges on the broad faces and the edges of precipitates, both of which appear to involve the motion of kinks. This paper reports the results of complementary high-resolution electron microscopy (HREM) studies which were performed on similar γ' precipitates in the same samples used for Part I.

2. EXPERIMENTAL PROCEDURES

2.1 Sample Preparation

The material, heat treatment and electropolishing techniques were described in Part I. In addition, light ion-beam milling of the thin foils just prior to examination was found to facilitate high-resolution imaging by removing a thin surface oxide which inevitably formed during polishing. In order to minimize heating during this process, the foils were ion-milled and cooled in alternating 30 second intervals, using an accelerating voltage of 4 keV, 0.3 mA

maximum total gun current and a 12° tilt.

2.2 High-Resolution Electron Microscopy

Lattice fringe imaging was performed on a Siemens 102 operating at 100 keV, using either the central spot or outer rings of an undersaturated LaB_6 filament in order to maximize beam coherence.^{1,2} The desired area was tilted to a $\langle 110 \rangle$ orientation and a systematic row of $\langle 111 \rangle$ reflections excited. After correction of astigmatism, an 0.28 \AA^{-1} objective aperture was positioned symmetrically around the forward scattered beam and the illumination was tilted so that this, and the proper $\langle 111 \rangle$ Bragg scattered beam were symmetrically positioned inside the objective aperture. The magnification was then increased to 300 to 500 kX, and the proper focus condition established by superposition of bright and dark field images. A through-focus series was then taken in 220 \AA increments based upon this position. For the Siemens 102 at 100 keV, $C_s = 1.1 \text{ mm}$, $C_c = 1.6 \text{ mm}$ and thus, $\Delta z_{\text{minimum contrast}} = -230 \text{ \AA}$ and $\Delta z_{\text{Scherzer}} = -640 \text{ \AA}$.

Axial lattice images were taken on a JEOL 200CX microscope, equipped with a pointed LaB_6 filament and operating at 200 keV. The procedures above were followed except that the specimen was tilted into an exact $\langle 110 \rangle$ orientation. In addition, an objective aperture was sometimes used to filter out higher order spatial frequencies and thereby, improve image contrast. After correction of astigmatism, the desired magnification was selected and a through-focus series was taken in 340 \AA increments, starting near the minimum contrast condition and continuing through Scherzer focus and the second pass-band interval. For the JEOL 200CX at 200 keV, $C_s = 1.2 \text{ mm}$, $C_c = 1.4 \text{ mm}$

and therefore, $\Delta z_{mc} = -240 \text{ \AA}$, $\Delta z_{Sch} = -660 \text{ \AA}$ and $\Delta z_{2nd} = -1290 \text{ \AA}$. Amorphous edges were included in the images whenever possible, and the angle of divergence was recorded on the electron diffraction patterns.

2.3 Optical Diffraction and Simulation

Optical diffraction was performed on high-resolution micrographs in order to determine the contrast transfer function and spatial frequencies recorded in the image, and also to search for lattice parameter variations and ordering within the Ag-rich precipitates.³ Additionally, image simulations were performed on the optical bench by constructing a dot or "atom" model of a γ' or γ hcp precipitate in an Al matrix in a $[\bar{1}01]$ orientation. Al and Ag atoms were scaled according to their atomic scattering factors, i.e. 5.889 and 8.671,⁴ respectively, and positioned as black dots on a white background. When a negative of this model was reduced to 6.0 mm x 6.6 mm and placed in the optical bench, it produced a diffraction pattern and image which were suitably sized for photographing on 35 mm film, using objective and projector lenses with focal lengths of 30 mm and 50 mm, and f-stops of 0.9 and 2.8, respectively. Several experiments were performed with this model using various apertures and illumination conditions.

3. RESULTS

3.1 Lattice Fringe Images of Precipitate Faces

Figure 1(a) shows a lattice fringe image of two intercepting precipitates in the quenched and aged sample. The foil orientation is $\langle 110 \rangle$ and the horizontal precipitate is edge-on and about 95 \AA

thick. A number of ledges are visible on both faces of the precipitate and three of these ledges (enclosed) are enlarged in Figs. 1(b) through (d). In these figures, ledge heights of two, four and six $\{111\}$ planes, i.e. 2.3, 4.6 and 6.9 Å are visible, as indicated. In addition, the $\{111\}$ planes appear to be continuous across the edges of the ledges, although the exact locations of the edges is somewhat uncertain. The fact that the ledges are multiples of two atomic layers in height supports the proposal that growth occurs by passage of Shockley partial dislocations across the faces on every other $\{111\}$ plane. Furthermore, the multiple heights of these ledges agrees with the results of the previous contrast analyses, where Shockley partial dislocations appeared to interact, leading to unusual contrast behavior.

It is also evident from these figures that with strong, two-beam tilted illumination conditions, substantial Fresnel diffraction can occur at the interface between the Ag-rich precipitate and the matrix, obscuring the interphase boundary. In order to verify that the observed ledges were not due to this effect, or some artifact of sample preparation, the sample was tilted roughly 60° to a second $\langle 110 \rangle$ orientation so that the faces of the precipitate could be examined. Although the number of contrast conditions taken was insufficient to determine the Burgers vectors of the dislocation ledges, they were visible, as indicated in the BF images in Figs. 2(a) through (c), where the letters correspond to the enlargements in Fig. 1.

Figure 3 shows a second lattice fringe image, taken in the same sample as above. The three precipitates, labeled A, B and C, are from four to six $\{111\}$ planes thick, although Fresnel diffraction

again makes it somewhat hard to define the exact interphase boundaries at the faces. Notice the large variation in aspect ratios among the precipitates, i.e. 9:1, 20:1 and 35:1 for A, B and C, respectively. Aaronson et al.⁵ have roughly estimated the interfacial free-energies of coherent, semicoherent and disordered $Al_{\alpha}/Ag_2Al_{\gamma}$ interfaces in an Al-18 w/o Ag alloy as about 40, 130 and 350 erg/cm², respectively. Based on these estimates, the equilibrium aspect ratios of coherent and semicoherent precipitates should be about 9:1 and 3:1. However, it is apparent from the three early-stage γ' precipitates in Fig. 3 that they can deviate from the predicted aspect ratios very early in the growth process. Since the local environment around each of the three γ' precipitates should be similar, these observations suggest that the deviation from equilibrium is most likely due to constraints imposed by the ledge mechanism of growth, rather than by interfacial energy effects. However, also notice that the $\{111\}$ planes are continuous across the ends of the precipitates, indicating that the ends may also be largely coherent with the matrix and not disordered as treated in the above analyses. Hence the equilibrium aspect ratio should be 3:1 or less.

3.2 Lattice Images of Precipitates

Axial lattice images were also taken of several precipitates in the quenched and aged sample⁶ in a $\langle 110 \rangle$ orientation. Figure 4(a) shows an isolated precipitate about 150 Å thick at its center, and two intersecting precipitates of slightly greater thickness. For this image, an objective aperture of radius 0.74 Å⁻¹ was used to eliminate higher order spatial frequencies, as shown in the

corresponding electron diffraction pattern in Fig. 4(b). The heights of a number of ledges are indicated in Fig. 4(a), and several of these are enlarged in Figs. 5(a) through (d). From the enlargements, it is readily apparent that ledges are present on both faces of both precipitates, and that the ledges are multiples of two atomic layers in height, as in the previous lattice fringe images. In addition, four and six-plane ledges are most common on the faces and are present in relatively large numbers. This is in agreement with the previous contrast experiments, where $1/6 \langle 112 \rangle$ and $1/2 \langle 110 \rangle$ dislocation contrast was primarily observed, further indicating that multiple-unit ledges are quite common, and that a Shockley partial dislocation is the basic ledge unit.

Also notice that in Figs. 4(a) and 5(d), ledges on opposite faces of the single precipitate tend to lie across from one another, as seen in the previous contrast analyses. In addition, the terraces between the ledges are atomically flat and ledges on both faces are uniformly stepped-down as they approach the plate edge from its center, in the lower right corner in Fig. 4(a). These characteristics lead exactly to the overall precipitate shape predicted by the general theory of precipitate morphology⁷ for growth by ledges, as sketched in Fig. 6.

Another important feature in these micrographs is that the $\{111\}$ planes are continuous across the edges of the ledges. This implies that if atomic attachment occurs at the edges as thought, then attachment takes place across a largely coherent interface, at least in this orientation and direction, and not across a disordered

interphase boundary as previously envisioned. That attachment is occurring at the edges of the ledges is supported by the fact that the edges are often indistinct while the faces or terraces between ledges are generally sharply defined. Particularly good examples of this are given by the four and six $\{111\}$ plane ledges in Fig. 5, where opposite edges of ledges are labelled (a) and (b). While the edges of the ledges give variable contrast, the terraces appear atomically flat.

Part of the variable contrast at the edges may be due to the fact that the dislocations/ledges are not exactly parallel to the $\langle 110 \rangle$ electron beam direction. A linear Shockley partial dislocation lying along $\langle 110 \rangle$ should have sufficiently few kinks in a thin foil so that its true projection is seen.⁸ However, as a ledge bends away from a low-index $\langle 110 \rangle$ orientation, the density of kinks increases rapidly, i.e. refer to Fig. 2 in Part I, thereby complicating image interpretation. Since the migration rate of an interface usually increases with its diffuseness,⁹ it would seem that the indistinct edges of ledges with a high density of kinks should migrate far more rapidly than the sharply defined broad faces of the precipitate. In addition, because the image often varies significantly across the riser of a given multiple ledge, even though the overall strain field of the riser resembles that of a single dislocation in a contrast experiment, each dislocation in the ledge may have its own density of kinks and hence, sites of atomic attachment.

The edge of the single precipitate and the precipitate intersection in the top-left corner of Fig. 4(a) are enlarged in Figs. 7(a) and

(b). The structures of the precipitate edges in these figures show that the edges are composed of a number of the same two-plane ledges, stacked vertically or slightly behind one another. In addition, note the distinct serrated shape associated with the edge in Fig. 7(a). Several terminating fringes are also discernable in the precipitate at this edge, at the locations indicated. Such $1/3\langle 111 \rangle$ dislocation loops around the precipitate periphery, with Burgers vectors normal to the faces, may be necessary to accommodate lattice parameter changes associated with the prism planes in well-developed precipitates. Thus, while atomic attachment should also take place at kinks on the precipitate edges, just as at the edges of ledges on the faces, there may be additional misfit dislocations at the edges, which are necessary to accommodate lattice parameter changes along the c-direction of the precipitate.

The precipitate intersection in Fig. 7(b) further supports the contention that atomic attachment does occur at the edges of ledges, and that these precipitates do not thicken by a continuous growth process of single atom jumps across the faces as proposed by some authors.^{10,11,13} For example, notice that the horizontally-oriented precipitate in Fig. 7(b) is roughly ten $\{0001\}$ planes thicker on the right side of the impinging precipitate than on the left side. Clearly this difference would only occur if the interface was thickening by a ledge mechanism rather than by continuous normal growth. Also notice that ledges migrating on the right face of the impinging precipitate appear to have stopped short of the intersected face, possibly due to "soft impingement" of diffusion fields and to a lesser

extent, to repulsion of the Shockley partial dislocations on the two faces of the precipitates.¹⁵

Optical microdiffraction was performed on the large precipitate in a search for changes in lattice spacing. Figures 8(a) and (b) show optical diffractograms taken from the matrix only, and with the precipitate and matrix spots superimposed, respectively. A slight elongation of the $\langle 111 \rangle$ spots due to the precipitate is evident in (b), giving a corresponding decrease in lattice parameter of about 2.5% along the c-axis of the precipitate, which is about 0.5% larger than decreases given by Barrett et al¹⁶ and Mondolfo.¹⁷ In addition, notice the strong $\langle 0001 \rangle$ precipitate reflections halfway between the forward scattered beam and the $\langle 111 \rangle$ matrix reflections in Fig. 8(b). These spots are also present in the electron diffraction pattern and have been interpreted in the past as meaning that the precipitates are ordered.^{18,19} However, in this study, slight tilting away from an exact $\langle 110 \rangle$ orientation diminished the intensity of the reflections, suggesting that they may be at least partially due to double diffraction from the hcp precipitate. This is possible, as indicated in the $[101]_{A1} // [2\bar{1}\bar{1}0]_{\gamma}$ diffraction pattern in Fig. 8(c). These reflections lead to strong $\langle 0001 \rangle$ periodicities, evident throughout the lattice images.

Figure 9(a) shows a second axial lattice image taken in the same sample without using an objective aperture, as indicated by the electron diffraction pattern in Fig. 9(b). The corresponding optical diffractogram is shown in Fig. 9(c). Again, several ledges on the

precipitate are indicated; however, in this micrograph, the precipitate/matrix interphase boundaries are not as well-defined as in the previous case.

First, notice that at the point of intersection enlarged in Fig. 10(a), several ledges (arrowed) appear to have nucleated near the edge of the impinging precipitate, and started migrating back toward its center. Also, note that the four-plane ledge enlarged in Fig. 10(b) is migrating on the same plane as the ledges coming from the intersection. Therefore, these ledges are not uniformly stepped-up or down with respect to each other. A similar situation is seen for the ledges on the bottom face in the lattice fringe images in Fig. 1, also involving a precipitate intersection.

3.3 Atomic Model of γ' Precipitate

An atomic model of a γ' or γ precipitate was constructed in a $[\bar{1}01]$ matrix orientation, based on the information obtained from the previous conventional and high-resolution images. The model, shown in Fig. 11, assumes that the precipitate is disordered and that no relaxations have occurred around the Shockley partial dislocations. Actually, atom planes adjacent to the left Shockley partials on the top face would not be as closely spaced as shown. In addition, the 2% contraction in the c-direction and 0.5% expansion along the c-axis in the hcp precipitate have been neglected. However, even with these simplifications, the model is relatively accurate.

The first layer of hcp precipitate was formed by introducing one Shockley partial on a (111) plane. Subsequent hcp layers on the top face were created by introducing additional Shockley partials

of the same type on every other (111) plane. The bottom face of the precipitate was thickened by adding opposite Shockley partials on ($\bar{1}\bar{1}\bar{1}$) planes. Using this construction, Shockley partials on opposite faces have opposite signs and therefore, might be expected to interact¹⁵ as seen in the previous images. Such partials were often aligned in the model to concur with the images.

3.4 Optical Simulations of Lattice Images

The precipitate model in Fig. 11 was also used for image simulation experiments on the optical bench. Figure 12 shows the results from this analysis. The original negative is shown in Fig. 12(a). The optical diffraction pattern from this negative, and the image which resulted when all of the beams were allowed to recombine, is shown in Fig. 12(b). The original image is reproduced, with a slight loss in clarity and some distortion near the outer edges. Also notice that the $\langle 0001 \rangle$ reflections present in electron diffraction patterns due to double diffraction, are not present in the optical diffraction patterns. This is due to the two-dimensional nature of the optical bench experiment. Figures 12(c) through (e) show how the image changes when successively smaller objective apertures are placed in back-focal plane. Although some detail is lost, the true atom positions, including the more closely spaced dislocations are reproduced, even when an aperture which just allows the $\langle 200 \rangle$ reflections to pass through is used, i.e. Fig. 12(d). Since this condition approximates the resolution limit of the JEOL 200CX at Scherzer defocus, it indicates the manner in which the previous lattice images may represent the true structure. When the aperture size is reduced to the extent that it prevents phase

contrast from occurring and a BF image is formed, true atom positions are lost or blurred and/or somewhat displaced. However, structure factor contrast is greatly increased as shown by Fig. 12(e). Figure 12(f) shows a two-beam lattice fringe image similar to those in this study.

4. DISCUSSION

The high-resolution microscopy results verify unambiguously that growth of γ' precipitates occurs by lateral migration of Shockley partial dislocations on alternate $\{111\}$ planes, rather than by any type of continuous normal growth mechanism. Also, multiple-unit ledges were often seen, further supporting the deductions made as to the origin of contrast behavior associated with ledges in the conventional TEM study in Part I. They also show that isolated precipitates have the shape predicted by the general theory of precipitate morphology, i.e. they are atomically flat between growth ledges, and are uniformly stepped-down from the centers to the edges. However, much more can now be said about possible growth mechanisms of individual ledges, and the configuration of the precipitates and their edges.

First, notice the structure of the ledges in the model in Fig. 11. The $\{111\}$ planes are continuous across the edges of the ledges, as observed in the lattice images. In addition, examination of a single two-plane ledge shows that a structural rearrangement or shuffling of atoms is required on only the upper atom plane, since the Shockley partial dislocation terminates in this layer. Therefore, the lower atom plane is similar to the matrix in all directions, except for strains due to the terminating partial dislocation in the layer

above. Thus, substitutional diffusion of Ag across this position should be similar to volume diffusion of Ag in the matrix, and almost independent of ledge structure. This implies that structural factors such as kink density and disorder at the edges may have to be considered only for the upper atom plane in a single two-plane ledge; formation of the upper layer may thus limit the growth process. In addition, because the lower layer possesses the required structural arrangement for the hcp phase before the Shockley partial dislocation has passed, substantial compositional changes may occur in this layer prior to its incorporation into the precipitate. These factors need to be included in kinetic analyses if an accurate understanding and modeling of the growth process is to be developed on an atomic level.

Since the precipitate edges in Fig. 11 are also composed of these same two-plane ledges, the (111) planes are continuous across the edges as well. Hence, the precipitate edges should grow by a mechanism similar to that of the ledges on the broad faces. However, it should also be noted that $1/3 \langle 111 \rangle$ dislocation loops around plates, whose presence is suggested by the lattice image in Fig. 7(a), must be enlarged non-conservatively, by the addition of vacancies to permit dislocation climb. Also notice that the radii of the precipitate edges can be determined very accurately by HREM for use in kinetic analyses; and are seen to vary significantly from the ideal parabolic cylinder shape often used in such analyses.²⁰

It is also interesting to compare the shapes of the precipitate edges with models of different possible ways of transforming cubic close-packed planes into a hexagonal lattice,²¹ as sketched in Fig.

13. As shown in Fig. 13(a), if the fcc to hcp transformation is accomplished by passage of identically oriented Shockley partial dislocations of the same type on every other $\{111\}$ plane, then an overall shape change occurs. This distortion must be accommodated within the matrix, resulting in a very high strain energy at the precipitate edges. However, if the transformation is accomplished by using equal numbers of all three Shockley partials on $\{111\}$, as illustrated in Fig. 13(b), then a large shape change does not occur. Such an arrangement would be highly favored from a strain energy viewpoint and consequently, the Shockley partial dislocations might be stacked vertically rather than at an angle as in the previous case. The appearance of all three types of Shockley partials on the same faces of precipitates and the residual contrast associated with the precipitate edges in Part I is consistent with the latter scenario. Such an interface might then resemble the serrated precipitate edge in Fig. 7(a).

Lastly, Fig. 14 illustrates the different types and configurations of dislocations that have been observed on the faces and at the edges of γ' precipitate plates during the conventional and high-resolution TEM studies. These dislocations include: (1) single $1/6\langle 112 \rangle$ Shockley partial dislocation ledges on the precipitate faces, (2) multiple-unit ledges on the precipitate faces composed of interacting $1/6\langle 112 \rangle$ dislocation loops on alternate $\{111\}$ planes, (3) $1/6\langle 112 \rangle$ dislocation ledges stacked vertically at the precipitate edges, (4) $1/2\langle 110 \rangle$ and $1/6\langle 112 \rangle$ dislocation loops wrapped around the precipitates and extending across the faces, and (at least sometimes) (5) $1/3\langle 111 \rangle$ Frank

dislocation loops in the precipitates at the plate edges. The presence of these dislocations is consistent with the expected requirements for growth and the accommodation of misfit for γ' precipitates, and was revealed by a combination of conventional and high-resolution TEM imaging techniques.

5. CONCLUSIONS

The interfacial structure of γ' precipitate plates in an Al-Ag alloy was studied by conventional and high-resolution TEM in order to: (1) test the general theory of precipitate morphology proposed by Aaronson,⁷ and (2) further understand the atomic structure and growth processes of ledges. The results of this study are as follows:

1. Both lattice and lattice fringe images show that ledges on the faces of γ' precipitates are multiples of two $\{111\}$ planes in height, supporting the theory and previous conventional TEM observations^{22,23} that thickening of the precipitates occurs by lateral migration of Shockley partial dislocations on every other $\{111\}$ plane.

2. There is a strong tendency for single $1/6 \langle 112 \rangle$ dislocation ledges to interact, forming multiple-unit ledges. Conventional TEM results showed a prevalence of $1/2 \langle 110 \rangle$, or six-plane ledges; however, similar numbers of two, four and six $\{111\}$ plane ledges were observed in lattice and lattice fringe images. Such combining of ledges may have been responsible for the range of migration rates observed at a given reaction temperature on the faces of similar precipitates in a previous investigation.²³

3. Both the edges of precipitates and ledges on the edges are also composed of $1/6 \langle 112 \rangle$ partial dislocations, which align vertically or slightly behind one another along the precipitate periphery. In

addition, a serrated edge shape was also observed, whose origin may relate to a minimum strain energy configuration due to the interaction of all three types of Shockley partial dislocations on alternate $\{111\}$ planes.

4. The $\{111\}$ planes are continuous across the edges of ledges on precipitate faces, and predominantly continuous across the precipitate edges as well. This indicates that both types of interfaces are similar, largely coherent and thus, not disordered as treated in most current kinetic analyses.²⁴ Therefore, ledges on both the faces and edges of precipitates should grow by similar mechanisms of atomic attachment.

5. Lattice images prove that growth occurs by lateral migration of these ledges and not by continuous normal growth as proposed by some investigators.¹⁰

6. The terraces between ledges are atomically flat and ledges are uniformly stepped-down from the centers to the edges of isolated precipitates, leading to the overall shape predicted by the general theory of precipitate morphology. The ideal precipitate shape is violated, however, when precipitates intersect, thus causing nucleation of ledges near the edges of intersecting precipitates and/or on the faces of the intersected precipitates.

7. Optical microdiffraction of γ' precipitates shows a slight decrease ($\sim 2.5\%$) in the spacing of the basal planes as compared with octahedral planes in the matrix, agreeing with conventional TEM images which show vacancy-type strain fields associated with the precipitates.⁶ In addition, there is evidence that in thicker precipitates, $1/3 \langle 111 \rangle$

Frank dislocations may also be present at the edges in order to accommodate the interplanar spacing changes.

8. Nuclei of γ' presumably have the equilibrium aspect ratio predicted by the Wulff theorem; however, there is strong evidence that the precipitates deviate significantly from this ratio almost immediately upon entry into the growth stage, doubtless due to the ledge-wise nature of their growth.

9. Reflections of the $\langle 0001 \rangle$ type from γ' precipitates in $\langle 011 \rangle$ matrix orientations may be partially due to double diffraction and not totally to ordering as reported by some investigators.

10. Optical simulations using an atomic model of a γ' precipitate in a $[\bar{1}01]$ orientation were used to verify the results obtained from high resolution images. In addition, this model also indicates that the diffusion of Ag into the upper and lower planes in a two-plane ledge could be different, since the Shockley partial dislocation terminates in the upper plane.

ACKNOWLEDGEMENTS

The authors gratefully acknowledge U. Dahmen for many helpful ideas regarding ledge growth. This work was supported by the Director, Office of Energy Research, Office of Basic Energy Sciences, Materials Science Division of the U.S. Department of Energy under Contract No. DE-AC03-76SF00098. One of the authors (J.M.Howe) acknowledges partial support by National Science Foundation Grant No. DMR 81-19507 through the Carnegie-Mellon University Metals Research Laboratory, and support to H.I. Aaronson from this same source is also gratefully acknowledged.

REFERENCES

1. R. Gronsky, in Treatise on Materials Science and Technology: Experimental Techniques, 19B, p. 325, Academic Press, New York (1983).
2. J.C.H. Spence, Experimental High-Resolution Electron Microscopy, p. 93, Clarendon Press, Oxford (1981).
3. R. Sinclair, in Introduction to Analytical Electron Microscopy, p. 507, Plenum Press, New York and London (1979).
4. P.A. Doyle and P.S. Turner, Acta Cryst. A24, 390 (1968).
5. H.I. Aaronson, J.B. Clark and C. Laird, Met. Sci. J. 2, 155 (1968).
6. J.M. Howe, H.I. Aaronson, and R. Gronsky, Acta Met., preceding article.
7. H.I. Aaronson, in Decomposition of Austenite by Diffusional Processes, p. 387, Interscience Publishers (1962).
8. A. Olsen and J.C.H. Spence, Phil. Mag. A. 43(4), 945 (1981).
9. J.W. Christian, The Theory of Transformations in Metals and Alloys, p. 499, Pergamon Press, Oxford (1965).
10. M. Ferrante and R.D. Doherty, Scripta Met. 10, 1059 (1976).
11. Y.H. Chen and R.D. Doherty, Scripta Met. 11, 725 (1977).
12. H.I. Aaronson, Scripta Met. 11, 731 (1977).
13. R.D. Doherty, M. Ferrante and Y.H. Chen, Scripta Met. 11, 733 (1977).
14. H.I. Aaronson, Scripta Met. 11, 741 (1977).
15. W.T. Reed, Dislocations in Crystals, p. 131, 128, McGraw-Hill, New York (1953).

16. C.S. Barrett, A.H. Geisler and R.F. Mehl, Trans. Met. Soc. AIME 143, 134 (1941).
17. L.F. Mondolfo, Aluminum Alloys: Structure and Properties, p. 213, Butterworths, London (1979).
18. J.A. Hren and G. Thomas, Trans. Met. Soc. AIME 227, 308 (1963).
19. R.B. Nicholson and J. Nutting, Acta Met. 9, 332 (1961).
20. R. Trivedi, Met. Trans. 1, 921 (1970).
21. P.G. Shewmon, Transformations in Metals, p. 274, McGraw-Hill, New York (1969).
22. J.A. Hren and G. Thomas, Trans. Met. Soc. AIME 227, 308 (1963).
23. C. Laird and H.I. Aaronson, Acta Met. 17, 505 (1969).
24. R. Trivedi, in Proceedings of an International Conference on Solid-Solid Phase Transformations, p. 547, The Met. Soc. AIME, Warrendale, PA (1982).

FIGURE CAPTIONS

- Fig. 1. (a) Lattice fringe image showing ledges on the face of a γ' precipitate oriented end-on, and (b) through (d) enlargements from Fig. 1(a) showing two, four and six $\{111\}$ plane heights of ledges.
- Fig. 2. (a) through (c) BF images of ledges after tilting specimen to observe face of precipitate; $[101]$ orientation.
- Fig. 3. Lattice fringe image of three early-stage γ' precipitates with aspect ratios of 9:1, 20:1 and 35:1 for A, B and C, respectively; $\langle 110 \rangle$ orientation.
- Fig. 4. (a) Low magnification lattice image of γ' precipitates with heights of ledges indicated, and (b) corresponding imaging condition used for lattice image; $\langle 110 \rangle$ orientation.
- Fig. 5. (a) through (d) Enlargements from Fig. 4(a) showing heights and structure of interfacial ledges.
- Fig. 6. Illustration of the ledge mechanism of growth and the precipitate shape predicted by the general theory of precipitate morphology (arrows indicate growth direction; stacking change also shown).
- Fig. 7. (a) and (b) Enlargements from Fig. 4(a) showing the structure of precipitate edges.
- Fig. 8. (a) Optical diffractogram from matrix only, (b) from matrix and precipitate, showing a slight elongation of the $[111]$ spot, and (c) superimposed diffraction patterns showing

appearance of $\langle 0001 \rangle$ reflections due to double diffraction from the hcp precipitate.

Fig. 9. (a) Second low magnification lattice image of γ' precipitates end-on, and (b) and (c) corresponding electron and optical diffraction patterns.

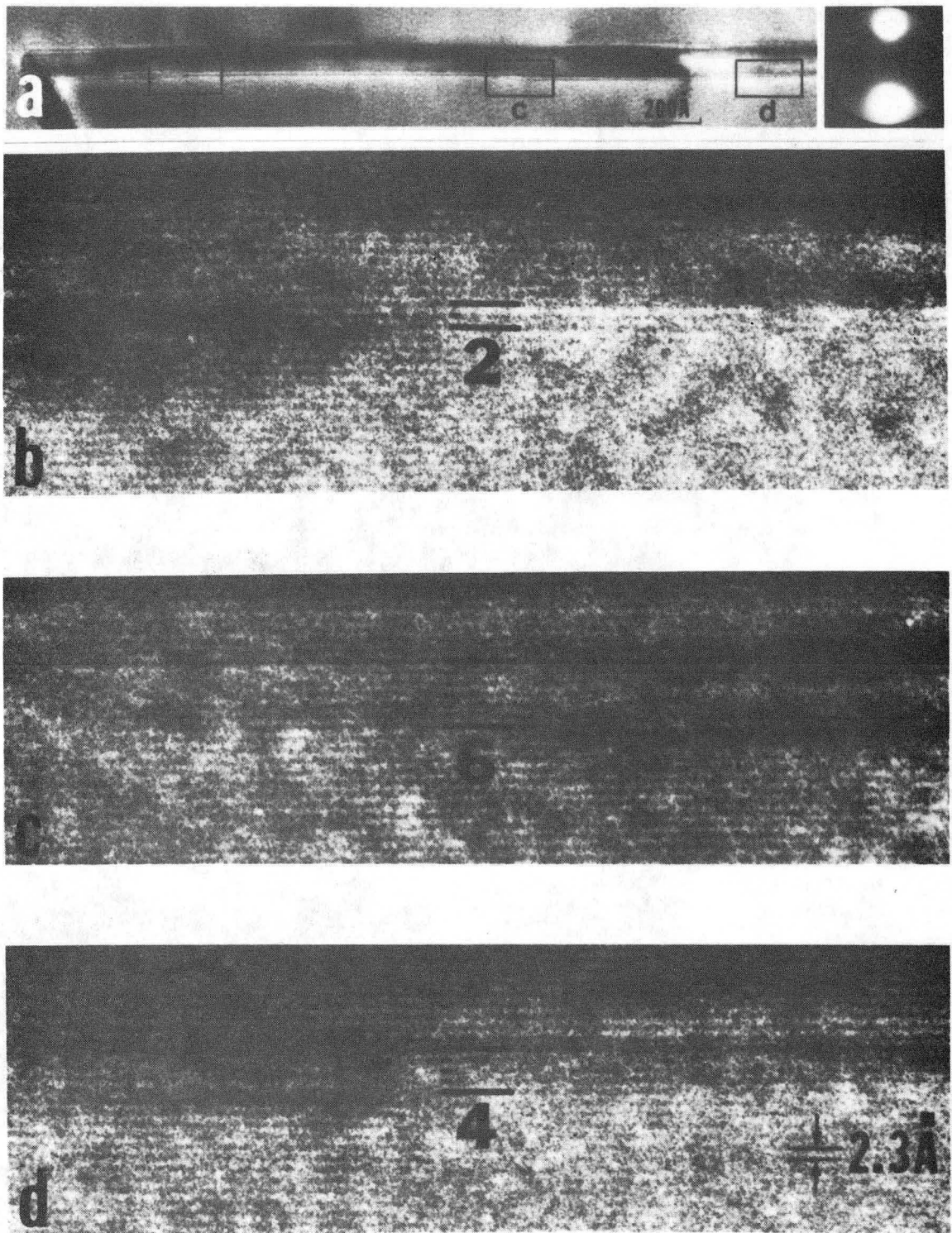
Fig. 10. (a) Enlargement from Fig. 9(a) showing ledges (arrows) near edge of impinging precipitate, and (b) enlargement showing four-plane ledge migrating on same plane as ledges coming from the precipitate intersection.

Fig. 11. Atomic model of a γ' precipitate formed by a passage of Shockley partial dislocations on every other (111) plane; paper normal is $[\bar{1}01]$ (see legend).

Fig. 12. Optical simulations of lattice images using the precipitate model in Fig. 11.

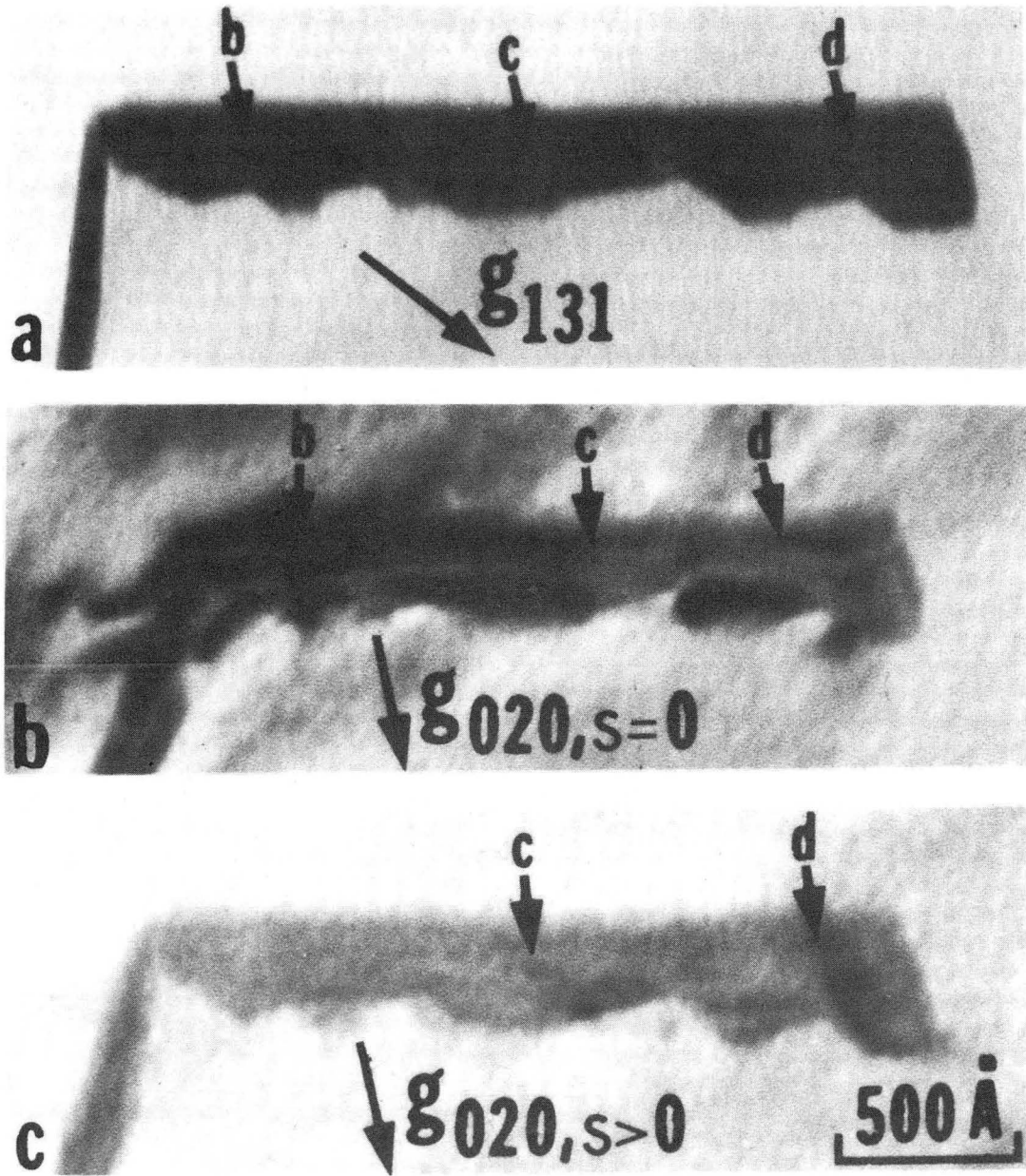
Fig. 13. Illustration of different ways of transforming cubic close-packed planes into hexagonal close-packed; (a) using only one Shockley partial, and (b) using equal numbers of all three Shockley partials.

Fig. 14. Summary of different dislocation configurations observed on γ' precipitates from conventional and high-resolution TEM studies.



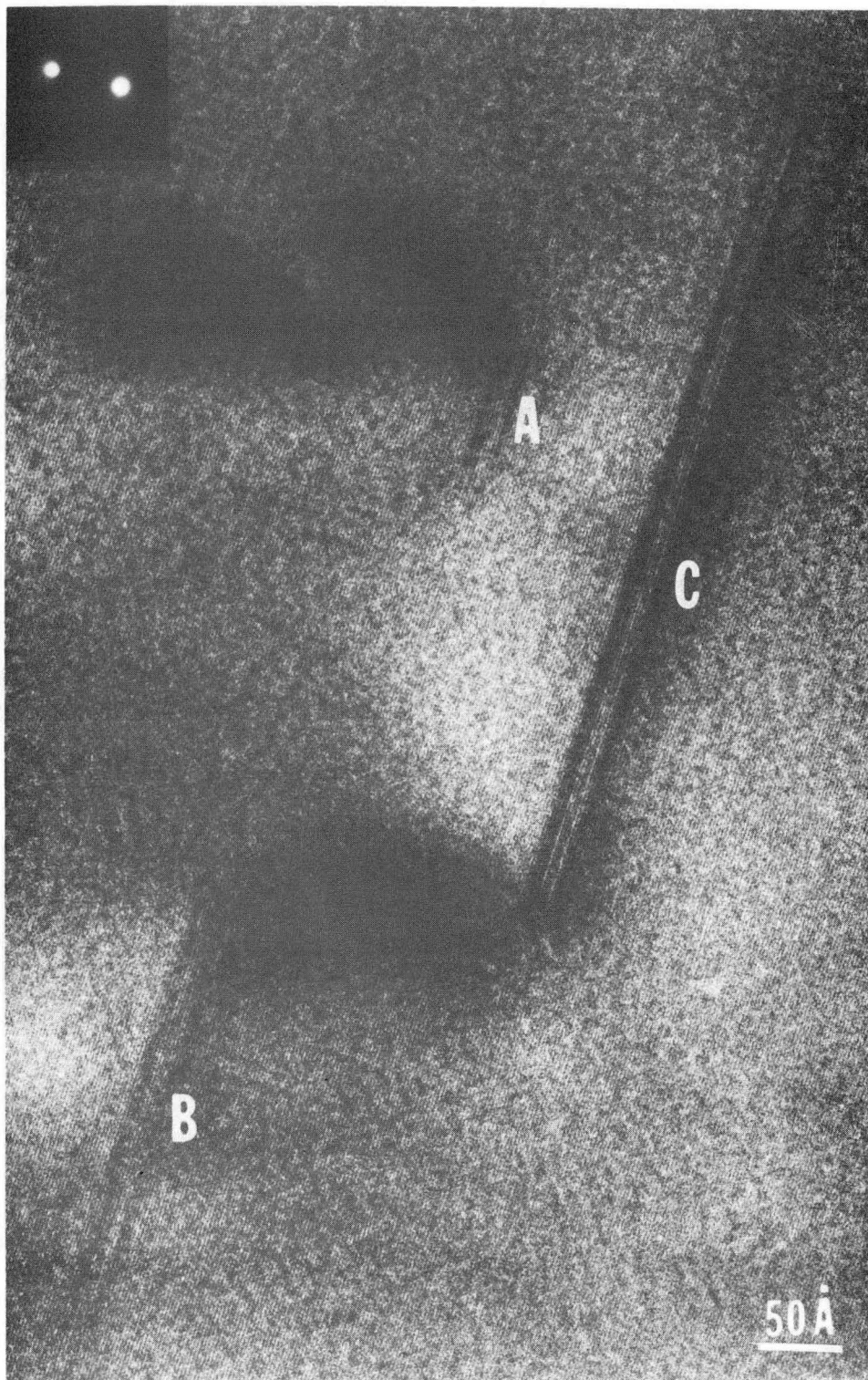
XBB 838-6698A

Fig. 1



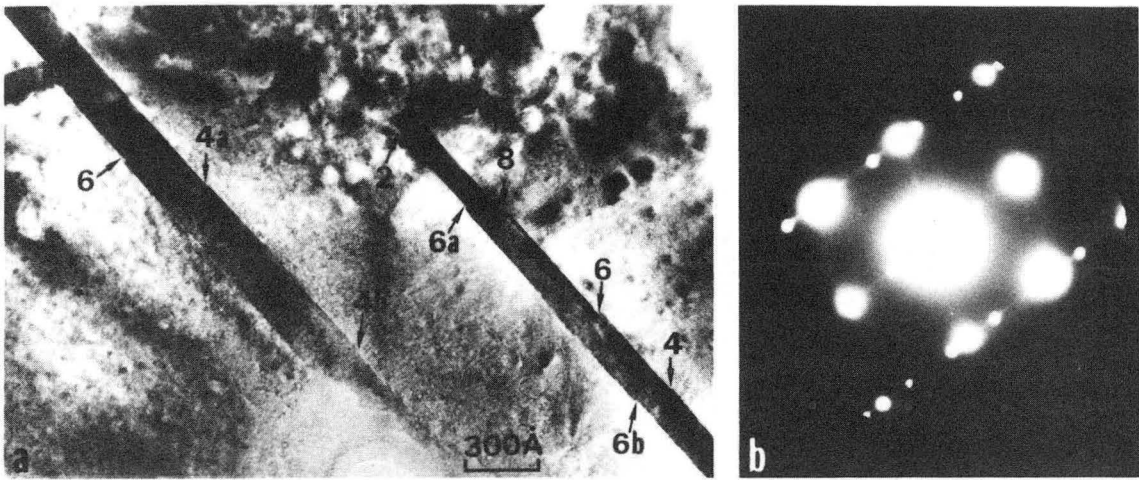
XBB 830-8824A

Fig. 2



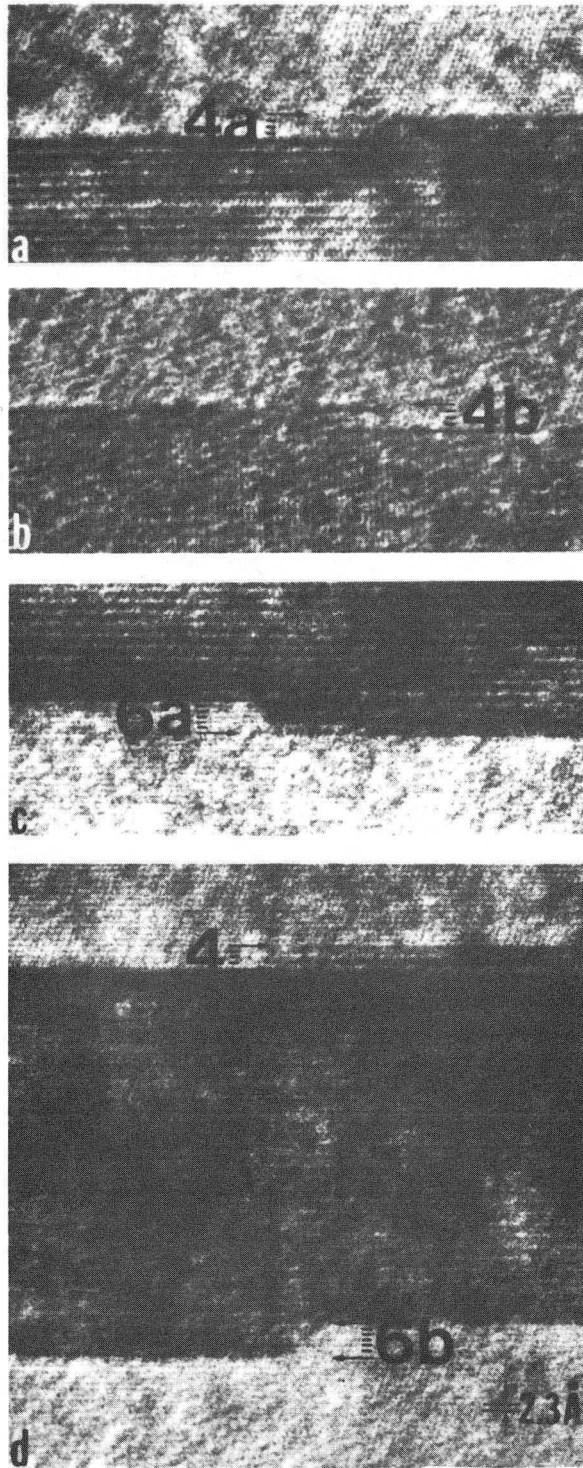
XBB 838-6700

Fig. 3



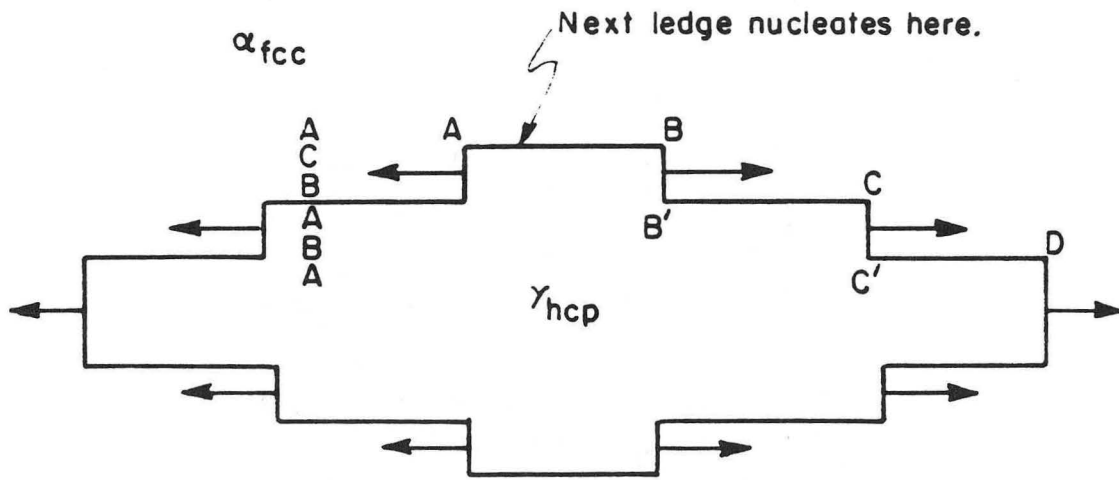
XBB 838-6710A

Fig. 4



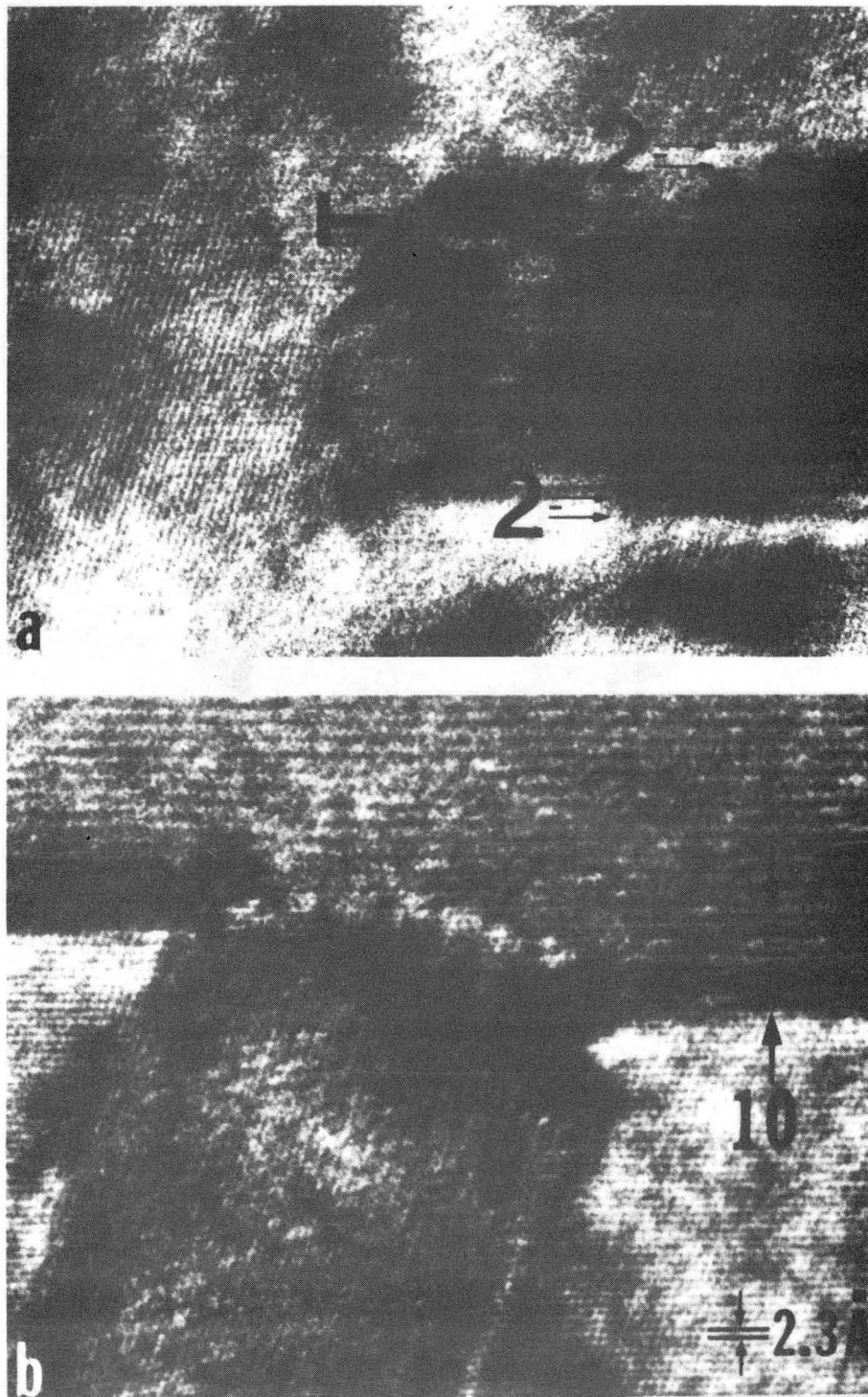
XBB 838-6702A

Fig. 5



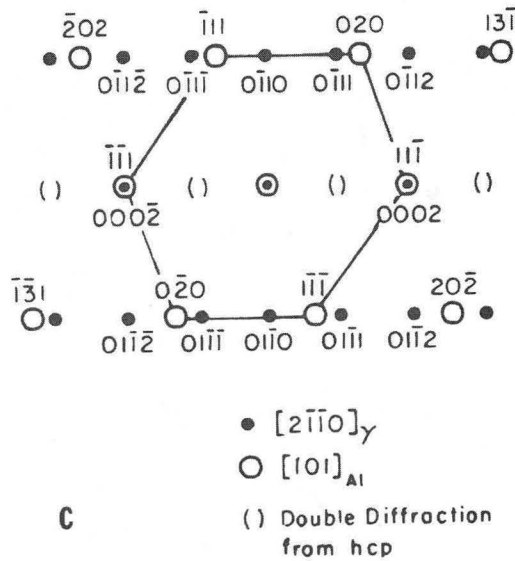
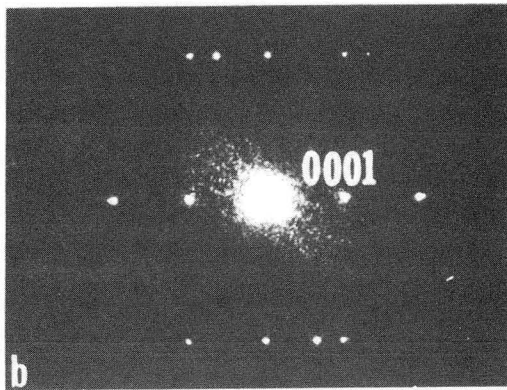
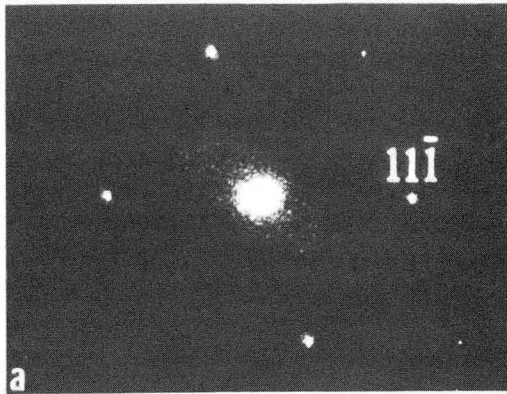
XBL 835-5706

Fig. 6



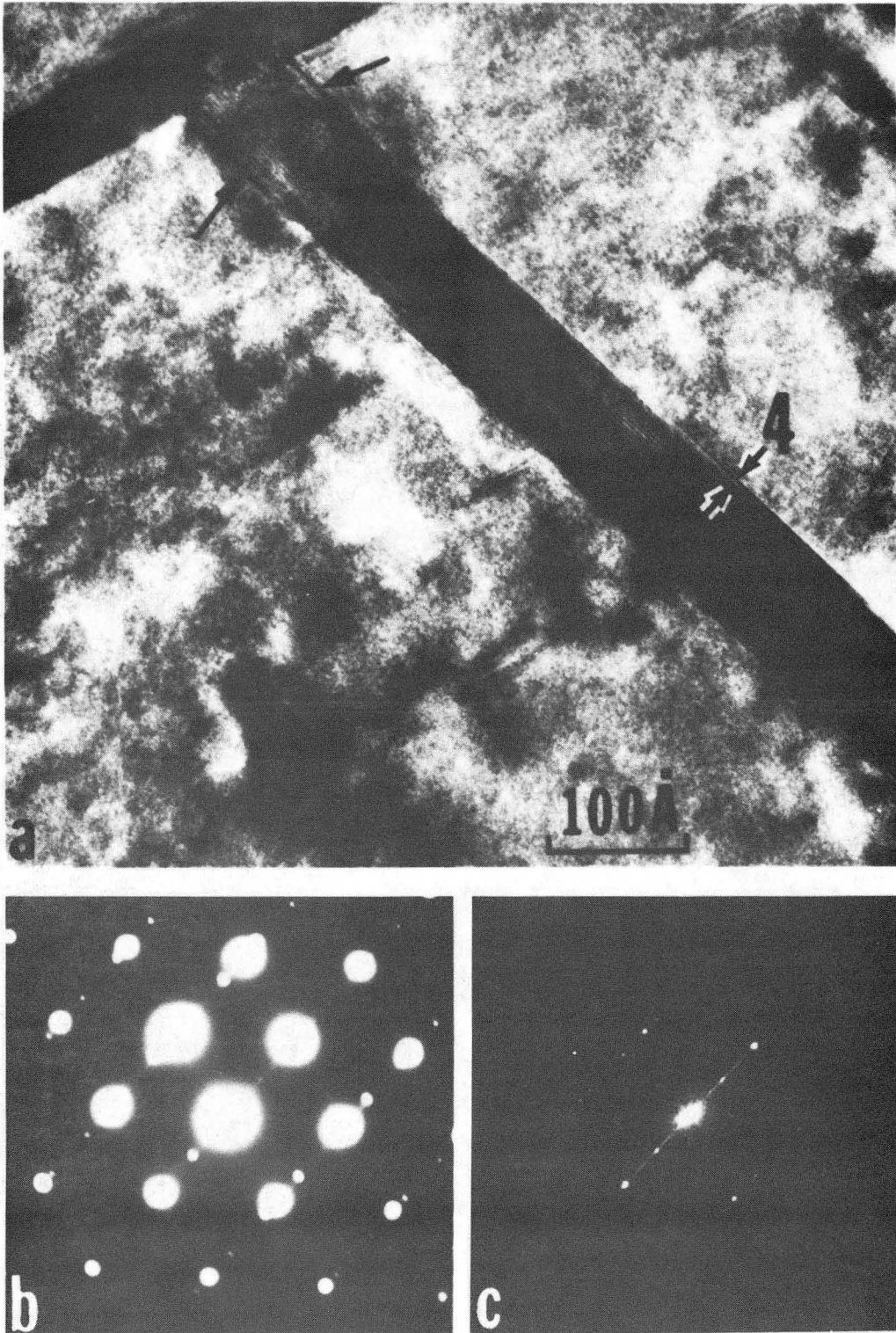
XBB 838-6699A

Fig. 7



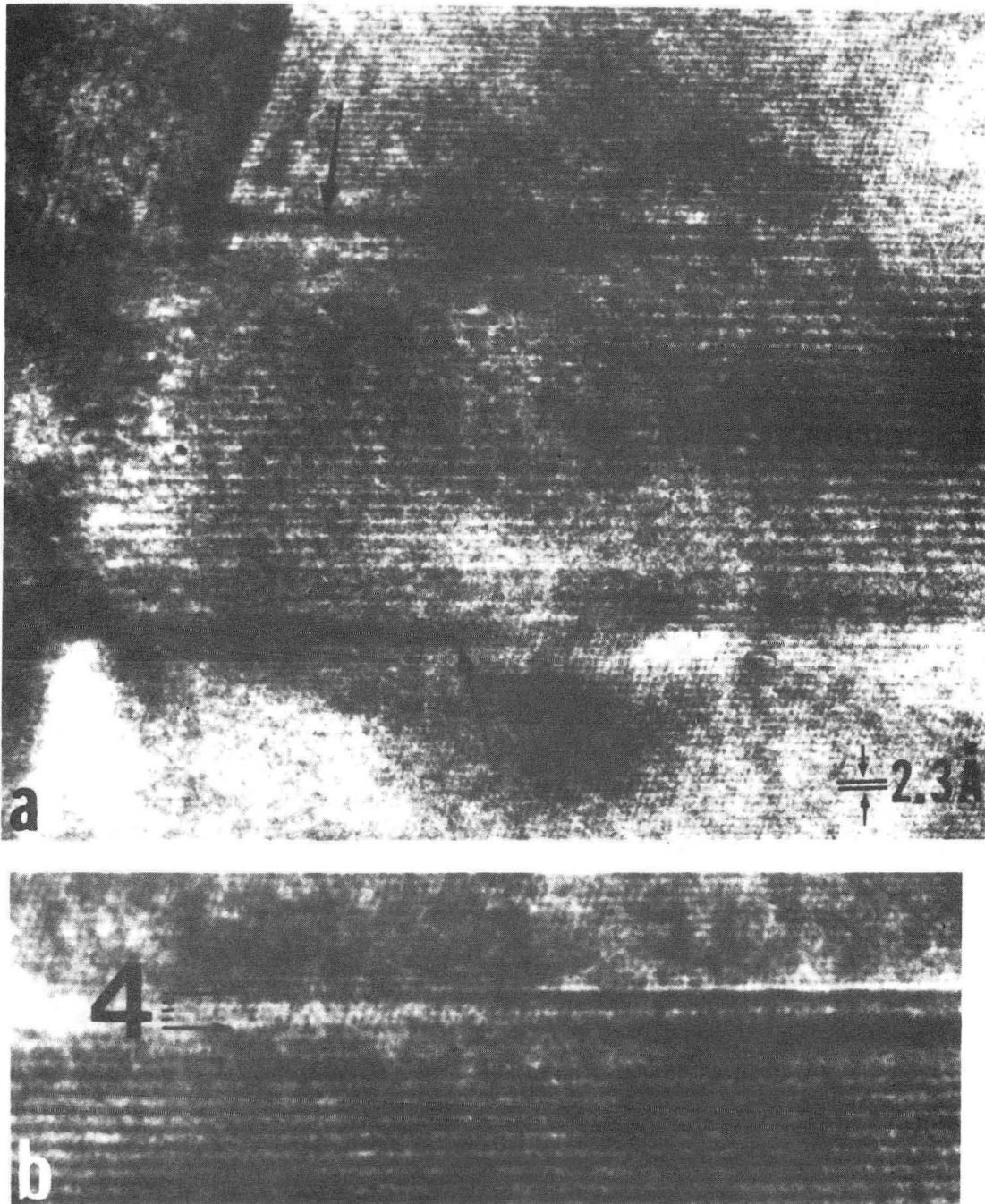
XBB 839-7850A

Fig. 8



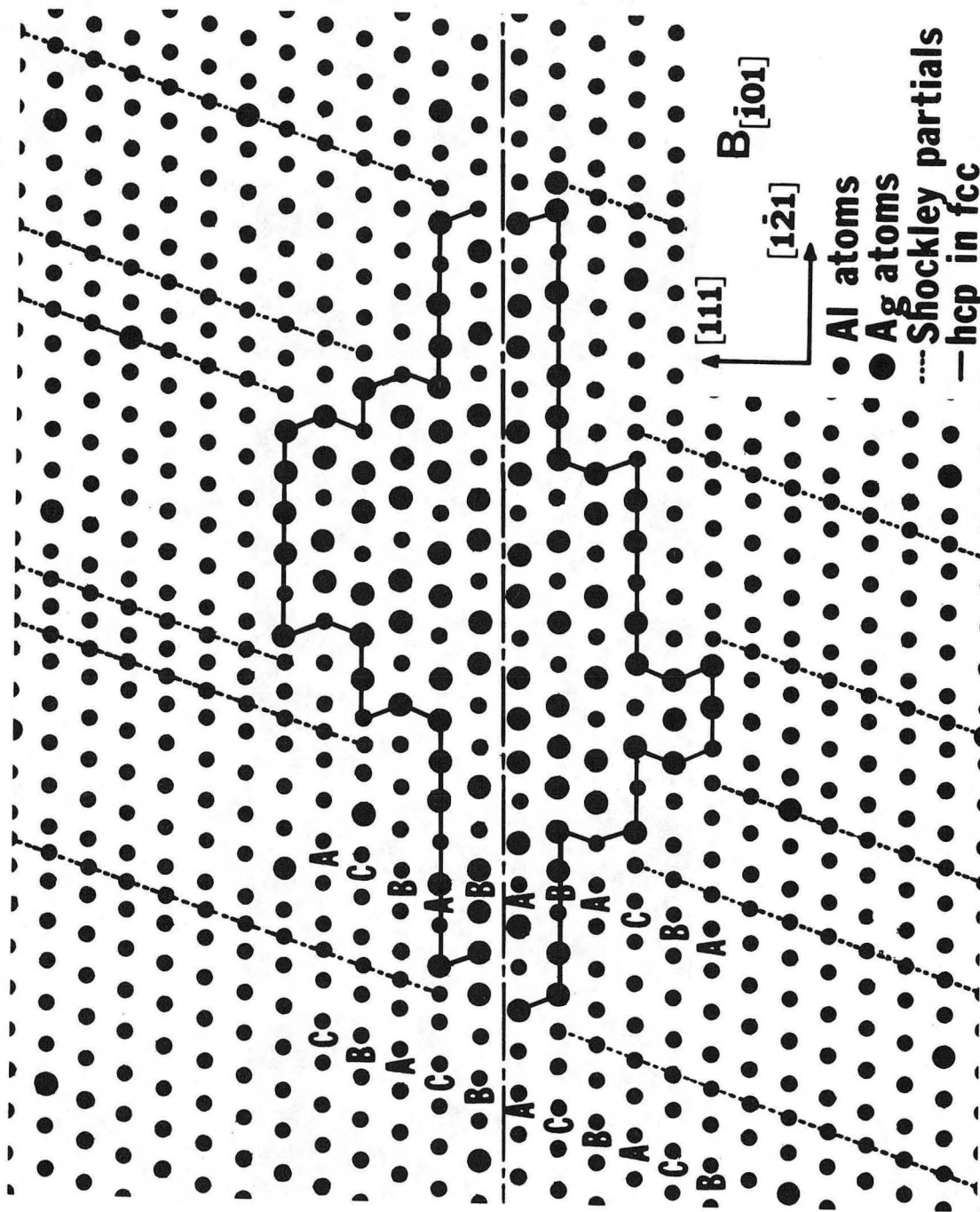
XBB 832-1591A

Fig. 9



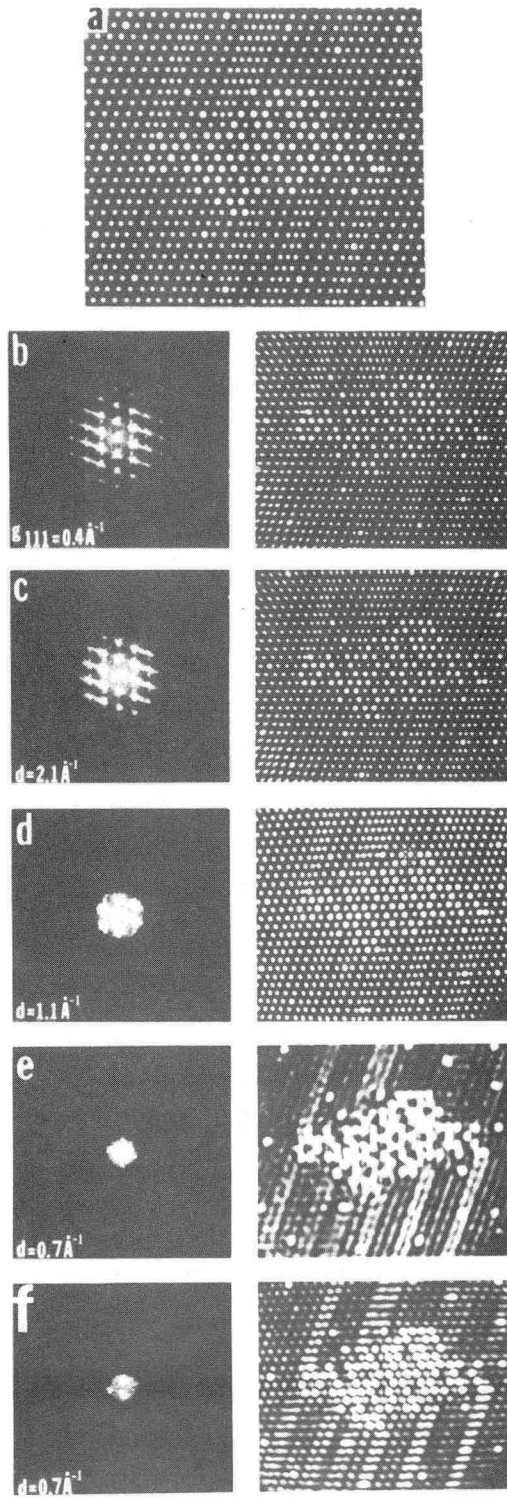
XBB 830-10554A

Fig. 10



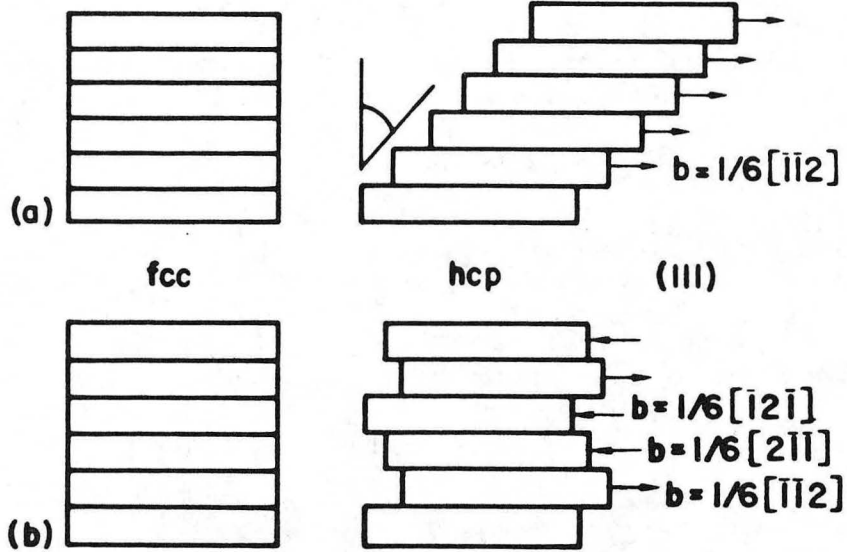
XBL 838-11075

Fig. 11



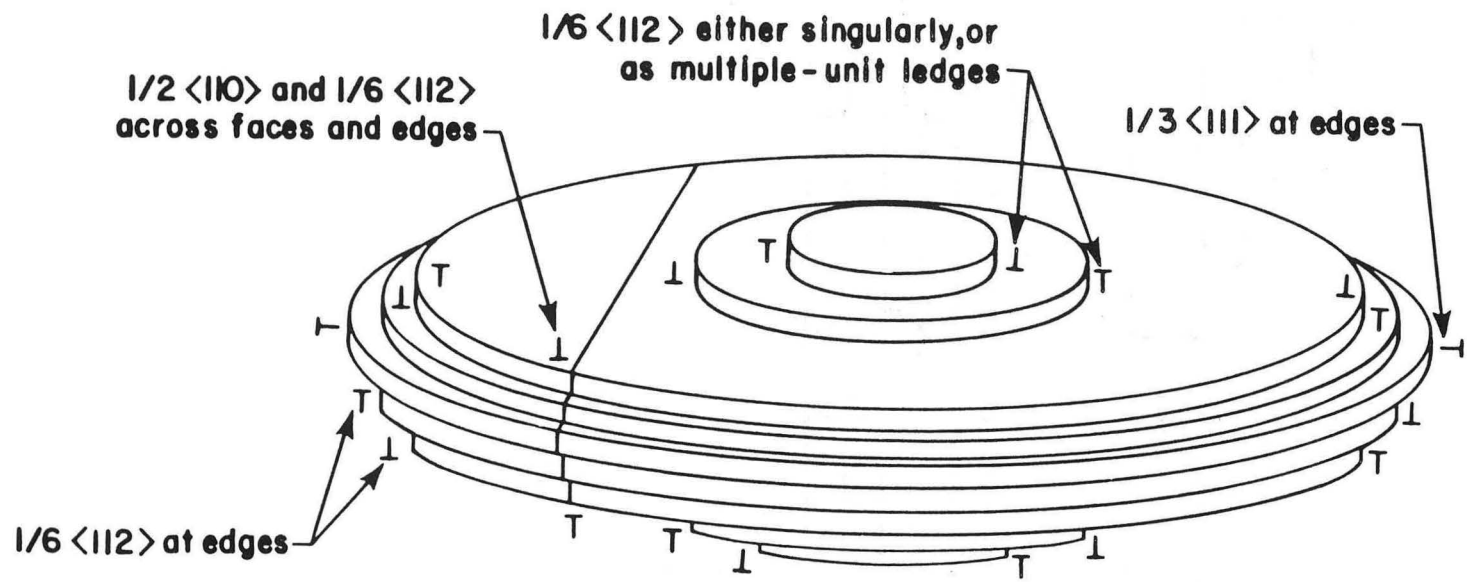
XBB 838-6708A

Fig. 12



XBL 841-10016

Fig. 13



XBL 841-10015

Fig. 14

This report was done with support from the Department of Energy. Any conclusions or opinions expressed in this report represent solely those of the author(s) and not necessarily those of The Regents of the University of California, the Lawrence Berkeley Laboratory or the Department of Energy.

Reference to a company or product name does not imply approval or recommendation of the product by the University of California or the U.S. Department of Energy to the exclusion of others that may be suitable.

TECHNICAL INFORMATION DEPARTMENT
LAWRENCE BERKELEY LABORATORY
UNIVERSITY OF CALIFORNIA
BERKELEY, CALIFORNIA 94720